

A Detailed Design Procedure for Printed Log-Periodic Antennas With Koch Fractal Dipoles

Arielly Rodrigues, Edson R. Schlosser and Marcos V. T. Heckler

Abstract—This paper presents a complete procedure for the design of printed log-periodic antennas. An investigation on the coaxial-to-parallel-strip transition usually present in this kind of antenna is discussed in detail and it is demonstrated to be very critical for the achievement of the desired impedance bandwidth. Furthermore, in order to reduce the overall antenna size, the dipoles have been implemented based on Koch fractals. It has been demonstrated that the use of Koch fractals allowed reducing the antenna area by 25 % in comparison to the classical printed log-periodic structure. Both designs have been optimized for the frequency range 2.3 – 6 GHz, so as to cover several wireless services, such as WLAN, mobile communications and WiMAX, among other applications. Experimental results validate the proposed design strategy.

Index Terms—Printed log-periodic antennas, Koch fractal, printed antennas.

I. INTRODUCTION

The increase of online services in the last years has changed everyone's life due to the wide availability of wireless communication access. Systems such as wireless local area network (WLAN), mobile communications of the fifth generation (5G) and worldwide interoperability for microwave access (WiMAX) are only few examples that are based on wireless technology. To access all these services simultaneously, a multiband or a wideband antenna (with fractional bandwidth larger than 10 %) must be used.

Several topologies of multiband antennas are available in the literature. Among others, the class of printed antennas are of special interest, since they exhibit several advantages such as low weight, ease of fabrication, low cost for mass production and flexibility in terms of polarization and input impedance [1]. Printed wideband end-fire topologies are available as well, such as the printed Yagi-Uda [2], the quasi-Yagi-Uda [3] and the printed log-periodic antenna [4], [5].

Printed log-periodic antennas have been already reported in the literature [6]–[8]. In [9], improvement of return loss has been achieved by soldering the coaxial cable only in the position of the coaxial-to-parallel-strip transition, whilst keeping the remaining part of the cable distant from the antenna itself. Additionally, a back ground plane has been added to the antenna, so as to allow isolation between the

radiator and the RF-circuitry. Another contribution has been presented in [10]. Although the parallel-strip transmission line has been analyzed, the design procedure yielded poor impedance matching in the upper part of the desired band.

Size reduction of printed log-periodic antenna has been also reported. The use of meandered dipoles has been described in [11], whereby an area reduction of 21% has been achieved. Antennas based on fractals have been studied by many authors and can be used to reduce the antenna dimensions or to obtain wideband or multiband operation. In [12], Koch fractals have been used for the first time for the design of printed log-periodic antennas. Both presented designs, using linear and fractal dipoles, yielded VSWR values larger than 2 in the desired band, even by using high-loss FR4 laminates. Koch fractals have been also used in [13]–[15]. All elements have been implemented with the same width, which does not respect the logarithmic periodicity. Moreover, the correct design of the parallel-strip transmission line used to feed the dipoles has not been considered in these publications.

The procedure to determine the lengths and distances between the elements of a standard log-periodic antenna (i.e. using wire elements) is well-known. However, for its printed version, special care must be taken for the feeding mechanism, which is normally accomplished by a coaxial-to-parallel-strip transition. To the best of the authors' knowledge, the influence of this transition on the impedance matching of printed log-periodic antennas has not been extensively reported in the open literature. For this reason, this paper presents a complete design procedure for optimum performance of printed log-periodic antennas implemented with straight and Koch fractal (used for antenna size reduction) dipoles. The next section is dedicated to describe the Koch fractal geometry. Section III presents the design procedure for the printed log-periodic antenna with linear dipoles. The same procedure is applied in section IV to design an antenna composed of dipoles of the first iteration of Koch fractals, so as to obtain an antenna with reduced size. It has been demonstrated that the use of Koch fractals allowed reducing the antenna area by 25 % in comparison to the classical printed log-periodic structure. Both designs have been optimized for the frequency range 2.3 – 6 GHz, so as to cover several wireless services, such as WLAN (2.45 GHz), 5G (2.6/3.5/5.2 GHz) and WiMAX (3.5/5.8 GHz) operating bands. They can be also applied as a compact auxiliary antenna for radiation pattern measurements in S-Band and in the lower half of the C-Band. Finally, section V presents validation of results with experimental data, whereby good agreement between simulated and measured results has been obtained.

Arielly Rodrigues was with Pillatel Serviços de Telecomunicações e Energia Eireli, Porto Alegre, Brazil, e-mail: ariellyrodrigues22@gmail.com, ORCID: 0000-0002-6888-3343.

E. R. Schlosser and M. V. T. Heckler were with Laboratório de Eletromagnetismo, Micro-ondas e Antenas - LEMA, Universidade Federal do Pampa - UNIPAMPA, Alegrete, Brazil, e-mails: edsonschlosser@unipampa.edu.br and marcos.heckler@unipampa.edu.br, ORCID: 0000-0001-5571-7728 and 0000-0002-6983-7760.

Digital Object Identifier: 10.14209/jcis.2024.2

II. THE KOCH FRACTAL

The Koch fractal has been introduced by Helge von Koch, as reported in [16], [17]. Its main feature is to transform a straight segment in four fragments with equal lengths, hence yielding a polygonal line. The first four iterations of the Koch fractal are shown in Fig. 1(a). The first iteration of the Koch fractal (K1) is detailed in Fig. 1(b). The original straight segment (K0) with total length l_0 is divided in three parts $l_0/3$ long. The central part is replaced by two segments with length $l_0/3$ in such a way as to form an equilateral triangle without the base. If one considers the K0 fractal with $l_0 = 1$ with the origin of a rectangular coordinate system positioned in the left point, then, for the fractal K1, it can be stated that:

- The segment C_1 exhibits no rotation nor translation.
- The segment C_2 presents rotation of 60° and translation of $l_0/3$ in the x -direction.
- The segment C_3 presents rotation of -60° and translation of $l_0/2$ in the x -direction and of $\sqrt{3}/6$ in the y -direction.
- The segment C_4 exhibits no rotation and translation of $2l_0/3$ in the x -direction only.

Hence iteration K1 is obtained by rotations and translations of a $1/3$ scaled version of the original straight segment K0 [15]. By using this procedure, the first iteration of the Koch fractal exhibits total length equivalent to $4/3$ of the original straight line.

The next Koch fractal iterations can be obtained by successively using these rotation and translation procedures of scaled versions of the former iteration. The second Koch fractal K2 is depicted in Fig. 1(c). It can be generated from fractal K1 when all the four segments are replaced by four new scaled versions of K1 by following the procedure outlined above. The K2 fractal exhibits total length equivalent to $16/9$ of the original K0. For the t -th iteration, the total length can be generalized to

$$l_t = \left(\frac{4}{3}\right)^t l_0. \quad (1)$$

III. DESIGN PROCEDURE FOR PRINTED LOG-PERIODIC ANTENNAS WITH LINEAR DIPOLES (K0)

As stated in section II, the Koch fractal K0 consists of a single straight segment. Hence the design procedure for the printed version is the same as for traditional log-periodic antennas except for the transformation of the cylindrical elements to flat strips.

The design begins with the specification of the desired operation band B , which has been specified to be within the range 2.3 – 6 GHz, and the desired directivity $D = 8$ dBi. For optimum operation, it has become a standard procedure to choose the optimum point on a constant-directivity contour for the log-periodic design. By doing so, the scale factor τ and the spacing factor σ for the log-periodic characteristic can be read from a plot originally presented in [18] and with corrections in [19]. With the chosen τ and σ values, the design band is normally corrected by

$$B_s = B_{ar} B, \quad (2)$$

where

$$B_{ar} = 1.1 + 7.7(1 - \tau)^2 \cot(\alpha) \quad (3)$$

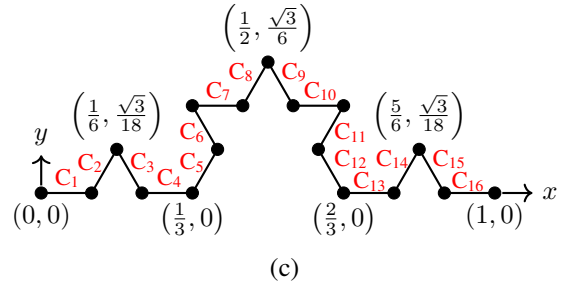
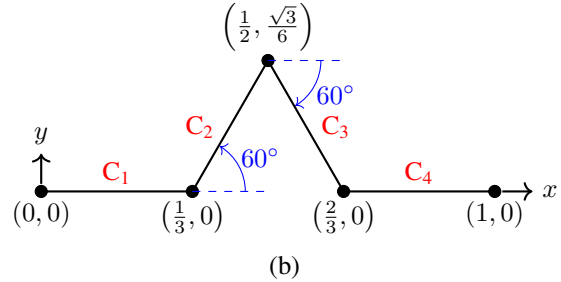
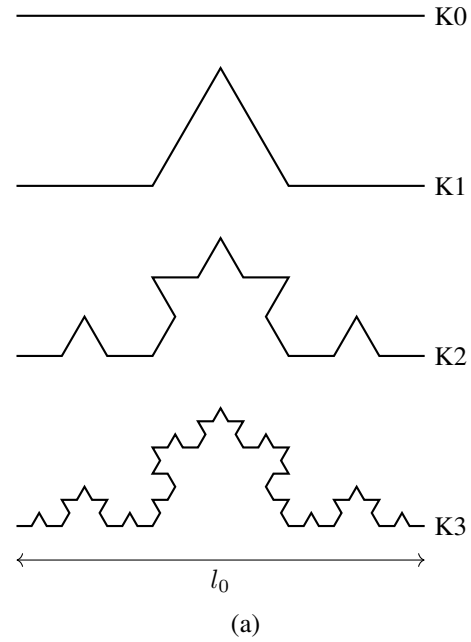


Fig. 1. (a) First iterations of the Koch fractal starting from a straight line (K0); (b) Detailed geometry of fractal K1; (c) Detailed geometry of fractal K2.

is the bandwidth of the active region of the antenna.

The total number of dipoles needed to fulfill the band and the directivity specifications is calculated by [19]

$$N = 1 + \frac{\ln(B_s)}{\ln(1/\tau)}. \quad (4)$$

The calculation of the dipole dimensions is based on the largest dipole. Its length is found by

$$l_N = 0.5\lambda_{max}, \quad (5)$$

with

$$\lambda_{max} = \frac{c_0}{f_{min}}. \quad (6)$$

The term c_0 is the speed of light in free space and f_{min} is the lowest frequency of the desired band B . The width of the largest printed dipole is obtained by [19]

$$W_N = \frac{\pi l_N}{e^{(2.25+z_a/120)}}, \quad (7)$$

where Z_a is the input impedance of the dipoles. In (7), the width W_N was found here by using the flat equivalent of a cylindrical dipole given in [20]. The spacing between the two largest dipoles is calculated by

$$S_N = 2\sigma l_N. \quad (8)$$

Finally, the dimensions of all the other dipoles can be determined by the recursive equation [19], [21]

$$\tau = \frac{l_{n-1}}{l_n} = \frac{S_{n-1}}{S_n} = \frac{W_{n-1}}{W_n}. \quad (9)$$

By using the formulation given above, the scale and the spacing factors for optimum operation were found to be $\sigma = 0.157$ and $\tau = 0.865$, respectively. These values allow calculating the angle

$$\alpha = \arctan\left(\frac{1-\tau}{4\sigma}\right), \quad (10)$$

which yields $\alpha = 12.13^\circ$. The total number of elements is $N = 11$ and the length of the largest dipole corresponds to $l_N = 65.217$ mm. By assuming $Z_a = 50 \Omega$, then $W_N = 14.236$ mm and the spacing between the largest dipole to the neighbor one is $S_N = 20.478$ mm. From these initial values and by using (9), the dimensions of the other antennas and the resulting values are summarized in Tab. I.

TABLE I
ANTENNA DIMENSIONS AND SPACINGS.

Dipole (n)	l_n (mm)	W_n (mm)	S_n (mm)
1	15.294	3.338	—
2	17.680	3.859	5.551
3	20.440	4.461	6.418
4	23.630	5.158	7.419
5	27.318	5.963	8.578
6	31.582	6.894	9.916
7	36.511	7.970	11.464
8	42.209	9.213	13.253
9	48.796	10.651	15.322
10	56.412	12.314	17.713
11	65.217	14.236	20.478

In the printed version of the log-periodic antenna, the transmission line used to feed the dipoles is a parallel-strip line. A cross-sectional view of this structure is shown in Fig. 2(a). Since this transmission line is balanced, the electric field distribution exhibits symmetric configuration with respect to the symmetry plane shown in Fig. 2(b). This means that the field distribution can be preserved if an infinite perfectly conducting plane is inserted exactly in the location of the symmetry plane, so as to preserve the Neumann boundary condition for the electric field \vec{E} , hence resulting in the equivalent structure composed of two isolated microstrip lines with half of the substrate thickness in comparison to the original parallel-strip transmission line, as illustrated in Fig. 2(c).

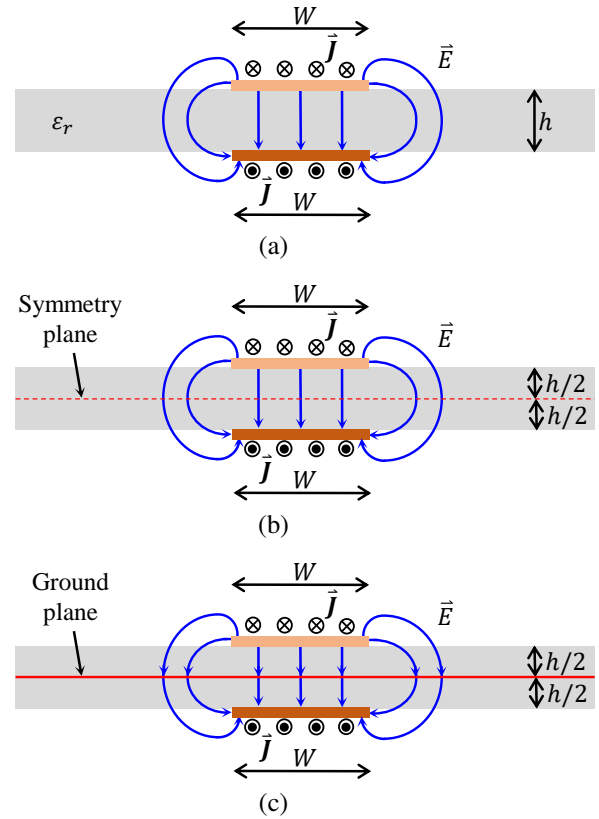


Fig. 2. Parallel-strip line and electric field distribution: (a) Parallel-strip transmission line; (b) Parallel strips with symmetry plane; (c) Isolated equivalent microstrip lines.

By using this analogy, the characteristic impedance can be calculated by [1]

$$Z_{0p} = 2Z_{0m}, \quad (11)$$

where Z_{0m} is the characteristic impedance of one of the equivalent microstrip lines shown in Fig. 2(c) and given by [1]

$$Z_{0m} = \frac{120}{2\sqrt{\epsilon_{re}}} \ln\left(\frac{F_1}{u} + \sqrt{1 + \frac{4}{u^2}}\right), \quad (12)$$

where

$$F_1 = 6 + (2\pi - 6)e^{-(30.66/u)^{0.7528}}, \quad (13)$$

$$u = \frac{W}{h/2}, \quad (14)$$

$$\epsilon_{re} = \frac{\epsilon_r + 1}{2} + \frac{\epsilon_r - 1}{2} \left(1 - \frac{10}{u}\right)^{-ab}, \quad (15)$$

$$a = 1 + \frac{1}{49} \ln\left(\frac{u^4 + (u/52)^2}{u^4 + 0.432}\right) + \frac{1}{18.7} \ln\left(1 + \left(\frac{u}{18.1}\right)^3\right) \quad (16)$$

and

$$b = 0.564 \left(\frac{\epsilon - 0.9}{\epsilon + 0.3}\right)^{0.053}. \quad (17)$$

In the equations above, the term ϵ_{re} is the effective dielectric constant of one of the equivalent microstrip lines, ϵ_r and h are the dielectric constant and the thickness of the laminate, respectively, and W is the width of the parallel strips.

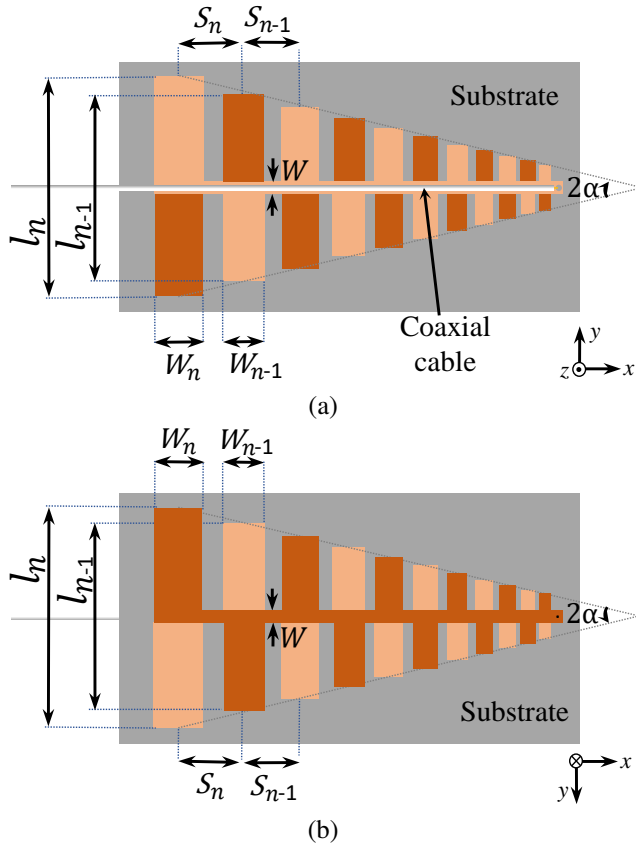


Fig. 3. Geometry of the printed log-periodic antenna with K0 elements: (a) Top view; (b) Bottom view.

For the frequency range 2.3 – 6 GHz and for the microwave laminate TACONIC TLC-338 with $\epsilon_r = 3.38$, loss tangent $\tan \delta = 0.0038$ and thickness of $h = 1.524$ mm [22], the use of equations (11)-(17) yields a parallel-strip line with $W = 4.5$ mm for a characteristic impedance $Z_{0p} = 50 \Omega$.

The resulting antenna geometry is illustrated in Fig. 3, whereby the external dimensions of the microwave laminate are 155 mm × 80 mm. The light and dark orange colors stand for metallizations printed on the top and bottom faces of the microwave laminate, respectively.

The next step is to design the antenna feeding point. For the printed antenna, this can be achieved by drilling a hole in the microwave laminate and etching a circle in the top strip to avoid short circuiting the inner and the outer conductors of the coaxial cable. Such a feeding topology has four main parameters: the radius of the etched circle R , the distance of the coaxial-to-parallel-strip transition from the smallest dipole L_c , the distance between the coaxial cable end to the drilled hole L_e , and the length of the open-ended stub L_s . These parameters are represented in Fig. 4. In order to assess the influence of each parameter on the input impedance matching, a set of parametric simulations has been carried out using the electromagnetic simulator Ansys HFSS.

The radius of the etched circle does not play an important role, provided that it is chosen sufficiently larger than the inner conductor radius of the coaxial cable, so as to avoid short-circuiting the coaxial cable end. Therefore, considering that the inner conductor radius of the coaxial cable is equal to

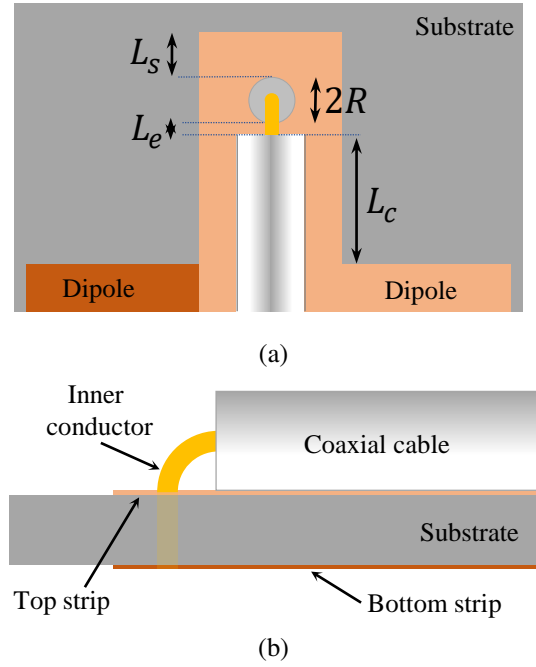


Fig. 4. Detailed view of the coaxial-to-parallel-strip transition: (a) Top view; (b) Cross-sectional view.

0.25 mm, the value $R = 0.75$ mm was chosen and will be kept fixed hereafter.

The parameter L_e should be kept ideally zero, since increasing the length of the inner conductor outside the coaxial line will introduce an additional and unnecessary inductive component into the antenna input impedance, hence affecting the overall impedance matching. However, small deviations from this ideal value may occur due to fabrication tolerances. Therefore, the parametric simulation was run by considering only small deviations from $L_e = 0.0$ mm, so as to assess the performance degradation and the results are shown in Fig. 5. It becomes clear that this parameter does not have strong influence on the impedance matching for small variations, which are typical of a reliable fabrication process.

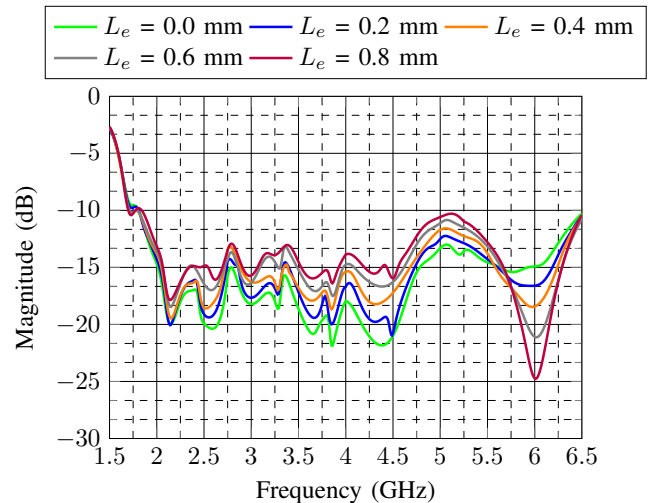


Fig. 5. Input reflection coefficient variation with the parameter L_e for the K0 printed log-periodic antenna.

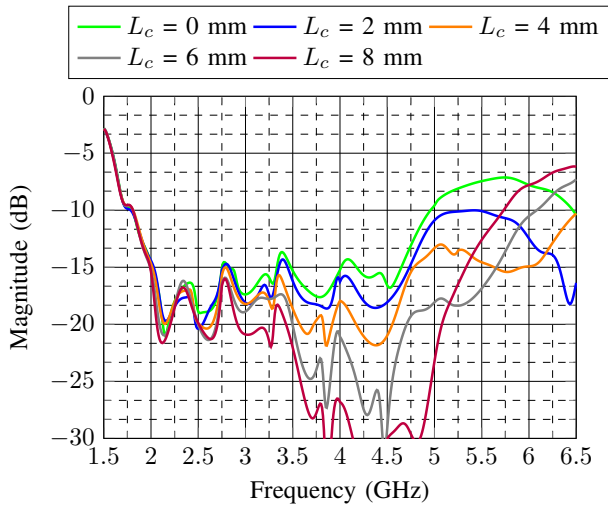


Fig. 6. Input reflection coefficient variation with the parameter L_c for the K0 printed log-periodic antenna.

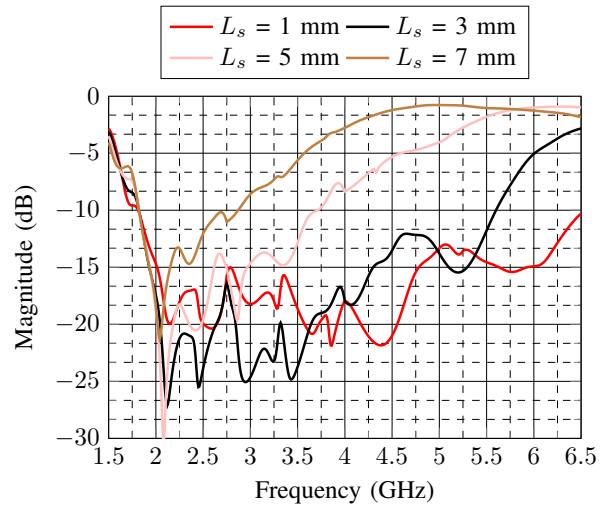


Fig. 7. Input reflection coefficient variation with the parameter L_s for the K0 printed log-periodic antenna.

The parameter L_c has been swept and the results are shown in Fig. 6. It becomes clear that this parameter plays an important role on the impedance matching, especially at the higher part of the analyzed band. Impedance mismatch in the higher part of the desired band has been also reported in [10], despite the correctness of the design procedure. In order to overcome this problem, the authors of [10] achieved improvement of impedance matching in the higher part of the frequency band by inserting an additional dipole between the transition and the original log-periodic array. In practice, this means to increase the design bandwidth and the overall antenna size to obtain acceptable performance, which is not suitable for antenna miniaturization purposes and can be avoided, provided proper optimization of the transition is carried out.

The fourth parameter of the transition, L_s , has also been varied and the results are shown in Fig. 7, where it becomes evident that this parameter has also strong influence on the impedance matching in the entire analyzed band. The main effect of this parameter is to introduce a capacitive component in the input impedance, which can be used to compensate the inductive behavior of the extension of the inner conductor of the coaxial cable. Since both L_c and L_s have strong influence on the impedance matching, a series of parametric simulations have been conducted by varying these two parameters simultaneously. The lowest overall reflection coefficient values in the range from 2.3 – 6 GHz have been obtained for $L_c = 4$ mm and $L_s = 1$ mm.

The influence of L_c and L_s on the input impedance matching can be further analyzed if the curves are plotted in the Smith chart. In Fig. 8, one can see that for both $L_c = 0$ mm and $L_c = 8$ mm, part of the data is outside the circle $|\Gamma| = -10$ dB, whereas nearly the complete frequency range is inside this circle for $L_c = 4$ mm. In Fig. 9, a large part of the curve is outside the circle $|\Gamma| = -10$ dB; this gets improved for lower values of L_s , which allows nearly the entire curve being inside the circle for $L_s = 1$ mm. These analyses indicate once again that there are optimum values for L_c and L_s that allow the antenna performance to be optimized in terms of impedance matching. In each Smith chart, only three curves

have been plotted for the sake of clear visualization of results.

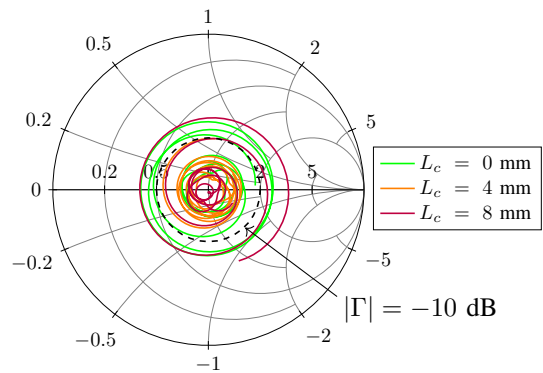


Fig. 8. Simulated reflection coefficient in the Smith chart as a function of L_c . The curves are plotted in the frequency range 2 – 6 GHz.

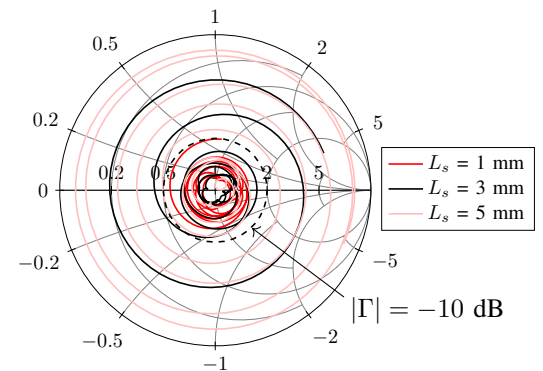


Fig. 9. Simulated reflection coefficient in the Smith chart as a function of L_s . The curves are plotted in the frequency range 2 – 6 GHz.

Finally, the simulated values for directivity were 8.6 dBi at both 2.4 GHz and 5.8 GHz, hence fulfilling the specified value at the beginning of the design. The simulated gain values are 8.2 dBi at 2.4 GHz and 8.0 dBi at 5.8 GHz, hence yielding radiation efficiency of roughly of 91 % and 87 %, respectively.

IV. DESIGN OF LOG-PERIODIC ANTENNAS WITH KOCH FRACTALS

Once the design procedure has been outlined for the printed log-periodic antenna with linear dipoles (K0), the same procedure has been applied by replacing the straight elements by Koch fractal of the first iteration (K1). This type of fractal should enable the log-periodic antenna to exhibit nearly the same electrical performance but with reduced dimensions.

The calculated dipole lengths must be distributed now with the K1 shape depicted in Fig. 1(b). The resulting geometry for this new antenna is presented in Fig. 10.

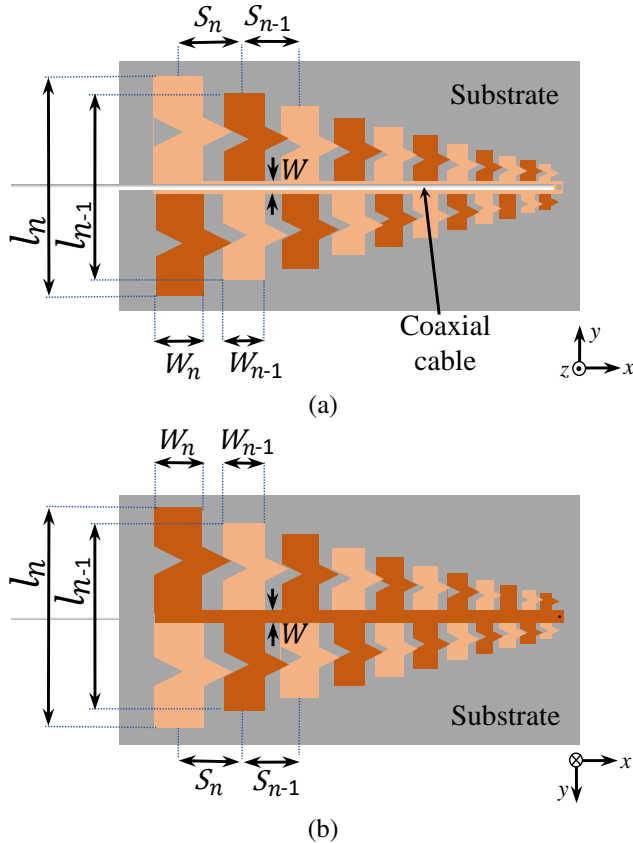


Fig. 10. Geometry of the printed log-periodic antenna with K1 elements: (a) Top view; (b) Bottom view.

The total antenna length is 157 mm and the width is 60 mm; hence the antenna composed of K1 dipoles yielded a microwave laminate area roughly 25 % smaller than for the antenna designed in the previous section with linear dipoles.

In order to optimize the input impedance matching, parametric simulations varying the parameters L_c and L_s have been performed also for this antenna. The results are shown in Fig. 11 for the former and in Fig. 12 for the latter. The general behavior of L_c and L_s is similar for both antennas with K0 and K1 dipoles. Nevertheless, it seems that L_c is less critical in this new design, since the impedance mismatch in the higher frequencies of the design band is not as poor as it was shown in Fig. 6. The optimization of the coaxial-to-parallel-strip transition has been carried out in the same way as for the antenna with linear dipoles. The parametric yielded $L_c = 4$ mm and $L_s = 1$ mm as the optimized values, which are the same found for the antenna with linear dipoles.

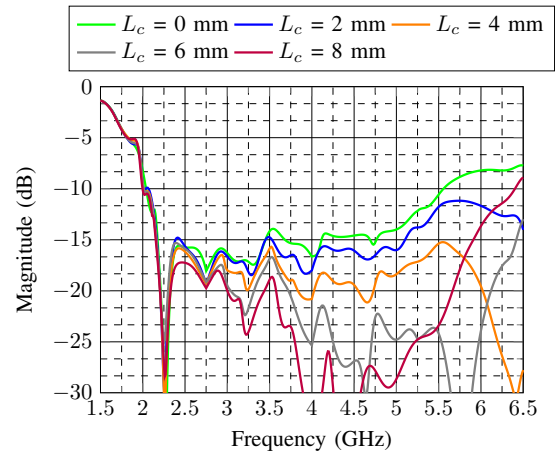


Fig. 11. Input reflection coefficient variation with the parameter L_c for the K1 printed log-periodic antenna.

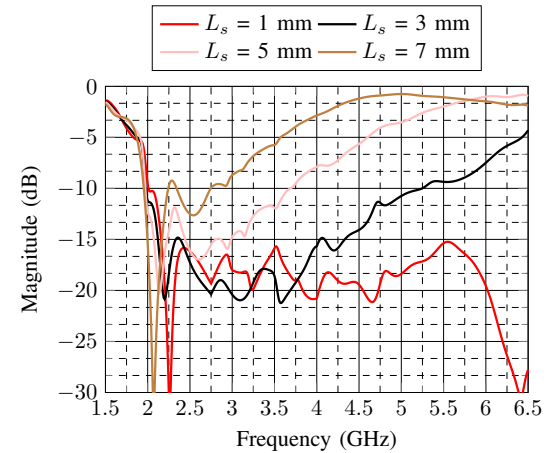


Fig. 12. Input reflection coefficient variation with the parameter L_s for the K1 printed log-periodic antenna.

The simulated directivity values for the antenna with K1 dipoles were 7.45 dBi at 2.4 GHz and 7.76 dBi at 5.8 GHz. The simulated gain values are 7.02 dBi at 2.4 GHz and 7.25 dBi at 5.8 GHz, hence yielding radiation efficiency of approximately 90 % and 89 %, respectively. The directivity and gain values are slightly below the ones for the antenna with K0 dipoles, because the antenna overall dimensions with K1 dipoles are smaller, hence resulting in a smaller effective length of the dipoles composing the log-periodic structure. The simulated gains for the designed antennas can be viewed in the Fig. 13.

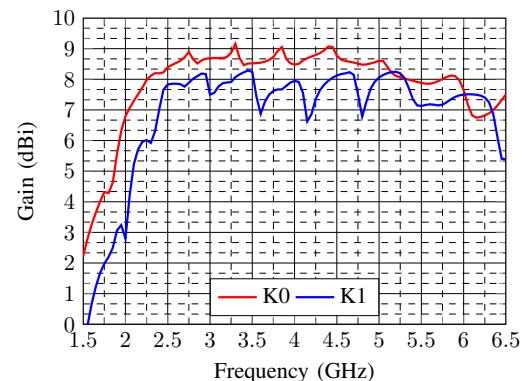
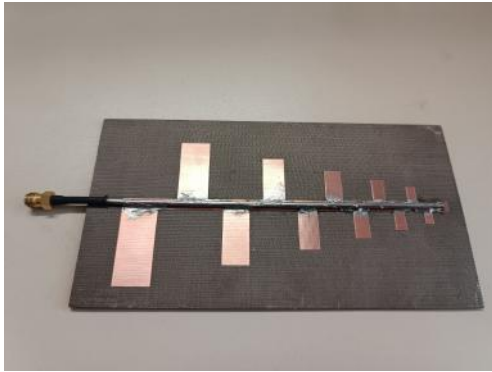


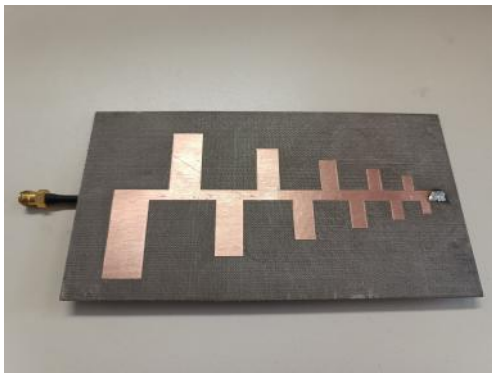
Fig. 13. Comparison between simulated gain versus frequency for the antennas designed with K0 and K1 elements.

V. VALIDATION

The designed antennas have been fabricated to validate the proposed design strategy. Fig. 14 presents the prototype of the antenna with K0 dipoles. The comparison between simulated and measured results for input reflection coefficient is shown in Fig. 15. Good agreement between the curves can be verified when a variation of $L_e = 0.6$ mm is considered. This deviation that occurred during the fabrication process.



(a)



(b)

Fig. 14. Prototype of the K0 printed log-periodic antenna: (a) Top view showing the coaxial cable soldered onto the top strip; (b) Bottom view showing the soldering at the feeding point.

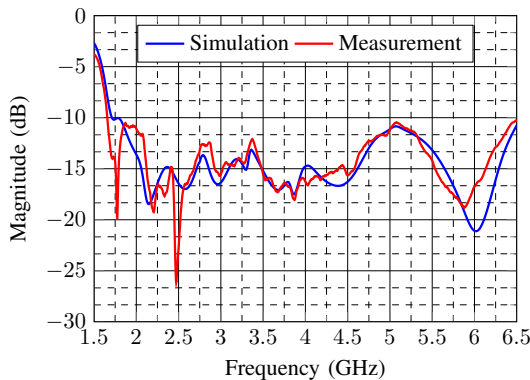
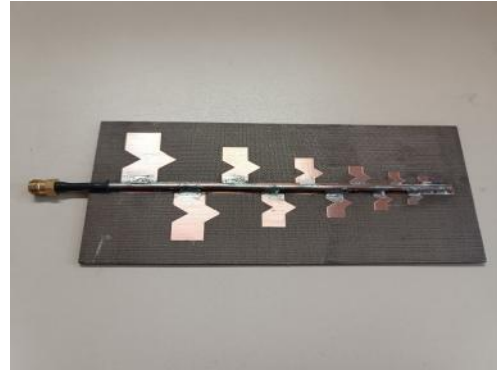


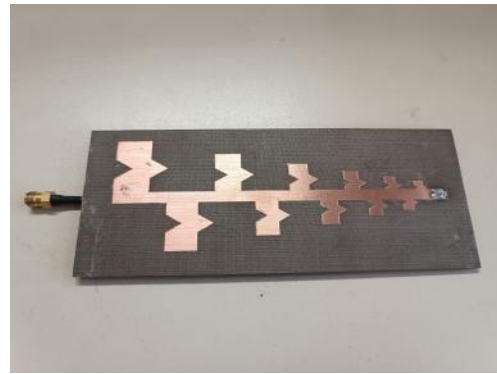
Fig. 15. Comparison between simulated and measured reflection coefficient versus frequency for the antenna designed with K0 elements.

Fig. 16 presents the prototype of the antenna with K1 fractal dipoles and the comparison between simulated and measured results for the input reflection coefficients is shown in Fig. 17. In this case, a fair agreement between the results has

been obtained. Nevertheless, the reflection coefficient remains below -10 dB in the entire design band, hence validating the proposed design.



(a)



(b)

Fig. 16. Prototype of the K1 printed log-periodic antenna: (a) Top view showing the coaxial cable soldered onto the top strip; (b) Bottom view showing the soldering at the feeding point.

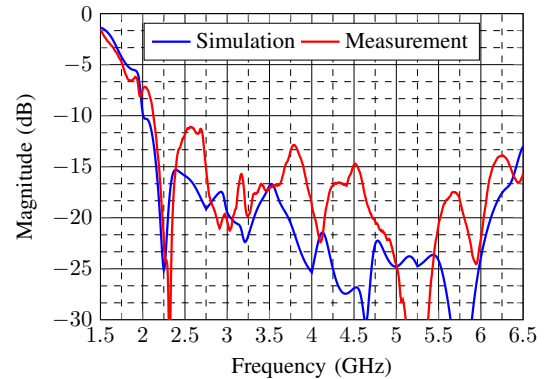


Fig. 17. Comparison between simulated and measured reflection coefficient versus frequency for the antenna designed with K1 elements.

Finally, the radiation patterns have been measured in a spherical near-field testing range. The antenna composed of K1 dipoles has been installed at the positioner and is shown in Fig. 18. In terms of radiation pattern, the performance for the antenna designed with K1 elements is demonstrated in Fig. 19 at 2.4 GHz and in Fig. 20 at 5.8 GHz.

Very good agreement between simulated and measured results can be verified. Some discrepancies can be observed in

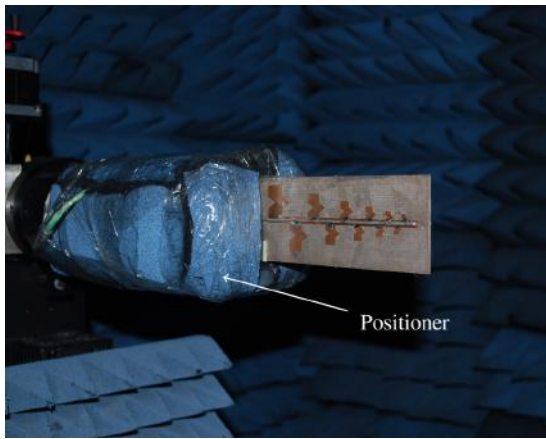


Fig. 18. Printed log-periodic antenna composed of K1 fractal dipoles installed in the spherical near-field testing range.

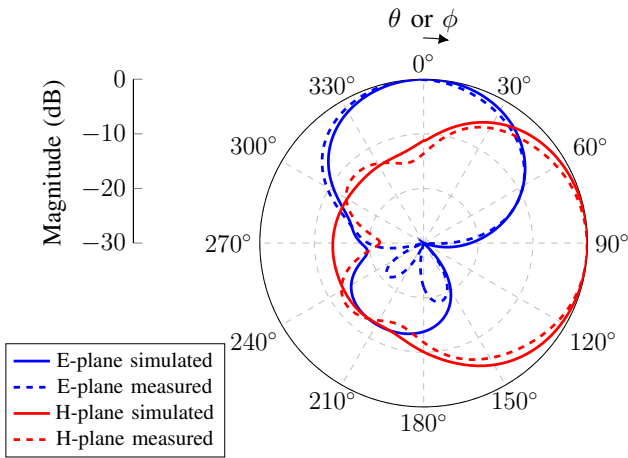


Fig. 19. Radiation patterns of the log-periodic antenna with K1 dipoles at 2.4 GHz. E-Plane: $E_{\phi}(\theta = 90, \phi)$, H-Plane: $E_{\phi}(\theta, \phi = 0)$.

the back region ($90^{\circ} \leq \phi \leq 270^{\circ}$ in the E-plane and $180^{\circ} \leq \phi \leq 360^{\circ}$ in the H-plane) and they are due to the measurement setup. The positioner used to install the antennas under test in the spherical near-field scanner caused the variations seen in the back of the antennas. However, it must be highlighted that excellent agreement has been obtained in the front part of the antenna.

From the 3D measured radiation pattern, the directivity values for the prototype could be estimated to be 8.05 dBi at 2.4 GHz and 7.86 dBi at 5.8 GHz, which are 0.6 dB and 0.1 dB above the simulated values, respectively. These results, along with the validation shown in Fig. 17, validate the design strategy proposed in this paper.

VI. CONCLUSION

A complete design procedure for printed log-periodic antennas has been described in this paper. The procedure has been applied for two different printed log-periodic designs: one with standard printed linear dipoles and the other with first iteration printed Koch fractal dipoles.

As the main contribution of this paper, it has been demonstrated that the level of reflection coefficient is strongly dependent on the coaxial-to-parallel-strip transition, which

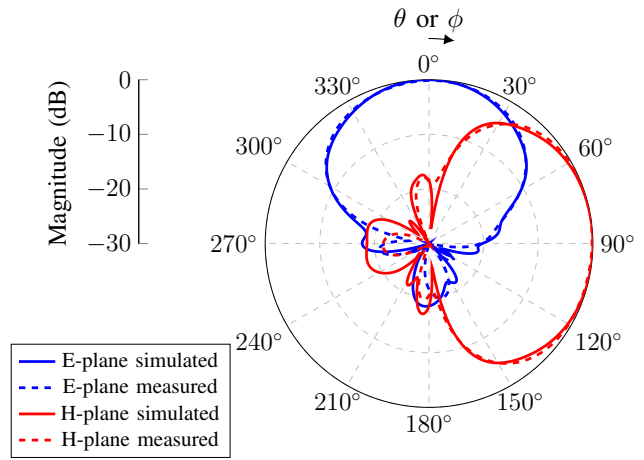


Fig. 20. Radiation patterns of the log-periodic antenna with K1 dipoles at 5.8 GHz. E-Plane: $E_{\phi}(\theta = 90, \phi)$, H-Plane: $E_{\phi}(\theta, \phi = 0)$.

is not considered in other papers available in the literature. This is particularly critical for the higher frequencies in the design band. In [12], the measured VSWR curves present values larger than 2.0 (reflection coefficient roughly larger than -10 dB) in the desired band. This behavior has not been observed in the measured results presented in this reference. In contrast to [10], the proposed approach demonstrated that there is no need to include more dipoles in the antenna, which increases the overall antenna length unnecessarily, provided that the coaxial-to-parallel-strip transition is properly designed. In comparison to [13]–[15], the results using the design methodology proposed in this paper yielded good impedance matching in a much wider band.

The agreement in terms of impedance matching and radiation pattern between numerical and experimental results is very good, hence validating the design strategy outlined in this paper.

The results presented in this paper indicates that both topologies can be successfully designed and fabricated. The antenna using the Koch fractal dipoles is indicated for applications that demand a compact wideband antenna. Additionally, the fractal-based printed log-periodic antenna allowed saving 25 % of laminate area. This is especially interesting for mass production.

REFERENCES

- [1] R. Garg, P. Bhartia, I. Bahl, and A. Ittipiboon, *Microstrip Antenna Design Handbook*. Ottawa, Ontario, Canada: Artech House, 2001.
- [2] B. K. Tehrani, B. S. Cook, and M. M. Tentzeris, "Inkjet printing of multilayer millimeter-wave yagi-uda antennas on flexible substrates," *IEEE Antennas Wireless Propag. Lett.*, vol. 15, pp. 143–146, 2016, doi: 10.1109/LAWP.2015.2434823.
- [3] Y. Qian, W. Deal, N. Kaneda, and T. Itoh, "Microstrip-fed quasi-yagi antenna with broadband characteristics," *Electron. Lett.*, vol. 34, no. 23, pp. 2194–2196, 1998, doi: 10.1049/el:19981583.
- [4] J. G. D. Oliveira, J. G. D. Junior, E. N. M. G. Pinto, V. P. S. Neto, and A. G. D'Assunção, "A new planar microwave sensor for building materials complex permittivity characterization," *Sensors*, vol. 20, pp. 1–15, 2020, doi: 10.3390/s20216328.
- [5] X. Wei, J. Liu, and Y. Long, "Printed log-periodic monopole array antenna with a simple feeding structure," *IEEE Antennas Wireless Propag. Lett.*, vol. 17, no. 1, pp. 58–61, 2018, doi: 10.1109/LAWP.2017.2773606.

- [6] G. Zhai, X. Wang, R. Xie, J. Shi, J. Gao, B. Shi, and J. Ding, "Gain-enhanced planar log-periodic dipole array antenna using nonresonant metamaterial," *IEEE Trans. Antennas Propag.*, vol. 67, no. 9, pp. 6193–6198, 2019, doi: 10.1109/TAP.2019.2924111.
- [7] Z. Hu, S. Cao, M. Liu, C. Hua, and Z. Chen, "A planar low-profile log-periodic array based on cavity-backed slot," *IEEE Antennas Wireless Propag. Lett.*, vol. 18, no. 10, pp. 1966–1970, 2019, doi: 10.1109/LAWP.2019.2933981.
- [8] D. Huang, G. Xu, D. Ding, W. Wang, L. Yang, Z.-X. Huang, X.-L. Wu, and W.-Y. Yin, "Wideband integrated log-periodic antenna array for 5G Q-band applications," *IEEE Antennas Wireless Propag. Lett.*, vol. 21, no. 7, pp. 1428–1432, 2022, doi: 10.1109/LAWP.2022.3170697.
- [9] A. Chauloux, F. Colombel, M. Himdi, J. Lasserre, and P. Pouliguen, "Low-return-loss printed log-periodic dipole antenna," *IEEE Antennas Wireless Propag. Lett.*, vol. 13, pp. 503–506, 2014, doi: 10.1109/LAWP.2014.2310057.
- [10] G. A. Casula, P. Maxia, G. Mazzarella, and G. Montisci, "Design of a printed log-periodic dipole array for ultra-wideband applications," *Prog. Electromagn. Res.*, vol. 13, pp. 15–26, 2013, doi: 10.2528/PIERC13012704.
- [11] A. A. Gheethan and D. E. Anagnostou, "Reduced size planar log-periodic dipole arrays (LPDAs) using rectangular meander line elements," ser. IEEE Int. Symp. Antennas Propagation (APS-URSI), San Diego - CA, 2008, doi: 10.1109/APS.2008.4619145.
- [12] D. E. Anagnostou, J. Papapolymerou, M. M. Tentzeris, and C. G. Christodoulou, "A printed log-periodic Koch-dipole array (LPKDA)," *IEEE Antennas Wireless Propag. Lett.*, vol. 7, pp. 456–460, 2008, doi: 10.1109/LAWP.2008.2001765.
- [13] V. S. Wildner and M. G. Vanti, "Koch fractal dipole antenna," ser. Brazilian Microwaves and Optoelectronics Symposium, Brazil, 2012 (in Portuguese).
- [14] —, "Design of Koch fractal log-periodic antenna with three Koch iterations for digital TV," ser. XXXI Brazilian Telecommunication Symposium, Brazil, 2013 (in Portuguese).
- [15] V. S. Wildner, "Development of fractal dipole and log-periodic antennas for digital TV: simulations and measurements," 2015, MSc. thesis, Universidade Regional de Blumenau, Brazil (in Portuguese).
- [16] K. J. Vinoy, J. K. Abraham, and V. K. Varadan, "On the relationship between fractal dimension and the performance of multi-resonant dipole antenna using Koch curves," *IEEE Trans. Antennas Propag.*, vol. 51, no. 9, pp. 2296–2303, 2003, doi: 10.1109/TAP.2003.816352.
- [17] D. H. Werner and S. Ganguly, "An overview of fractal antenna engineering research," *IEEE Antennas Propag. Mag.*, vol. 45, no. 1, pp. 38–57, 2003, doi: 10.1109/MAP.2003.1189650.
- [18] R. L. Carrel, "Analysis and design of the log-periodic dipole antenna," 1961, PhD thesis, University of Illinois.
- [19] C. A. Balanis, *Antenna Theory: Analysis and Design*. Wiley-Blackwell, 2005.
- [20] C. Campbell, I. Traoulay, M. Suthers, and H. Kneve, "Design of a stripline log-periodic dipole antenna," *IEEE Trans. Antennas Propag.*, vol. 25, no. 5, pp. 718–721, 1977, doi: 10.1109/TAP.1977.1141653.
- [21] J. A. J. Ribeiro, *Engenharia de Antenas: Fundamentos, Projetos e Aplicações*. Editora Erica, 2012.
- [22] *Taconic TLC specialty laminates*, Taconic, 2010.



devices based on lumped elements.

Edson R. Schlosser was born in Santa Rosa, Brazil, in 1989. He received the B.Sc. and M.Sc. degrees in electrical engineering from Universidade Federal do Pampa, Brazil, in 2011 and 2014, respectively, and the Ph.D. degree from Pontifícia Universidade Católica do Rio de Janeiro, Brazil, in 2020. Since 2013, he is professor at Universidade Federal do Pampa, Alegrete, Brazil. His current research interests are the design of microstrip antennas, arrays and reflectarrays, synthesis of radiation patterns using meta-heuristics, and design of passive microwave



Marcos V. T. Heckler (M06) was born in Rio Grande, Brazil, in 1978. He received the B.Sc. degree in electrical engineering (emphasis in electronics) from the Universidade Federal de Santa Maria (UFSM), Brazil, in 2001, the M.Sc. degree in electronic engineering (microwaves and optoelectronics) from Instituto Tecnológico de Aeronáutica (ITA), Brazil, in 2003, and the Dr.-Ing. (Ph.D.) degree from the Technische Universität München, Munich, Germany, in 2010. From April to August 2003, he worked as a Research Assistant with the Antennas and Propagation Laboratory, ITA, Brazil. From October 2003 to June 2010, he worked as a Research Associate with the Antenna Group, Institute of Communications and Navigation, German Aerospace Center (DLR), Oberpfaffenhofen, Germany. Since 2010, he is professor at Universidade Federal do Pampa, Alegrete, Brazil. His current research interests are the design of microstrip antennas and arrays, and the development of numerical techniques for microstrip antennas.



Arielly Rodrigues was born in Santa Rosa, Brazil, in 1994. She received the B.Sc. degree in telecommunication engineering from Universidade Federal do Pampa, Brazil, in 2018. Since 2018, she has been working as a bidding analyst and FTTx project manager.